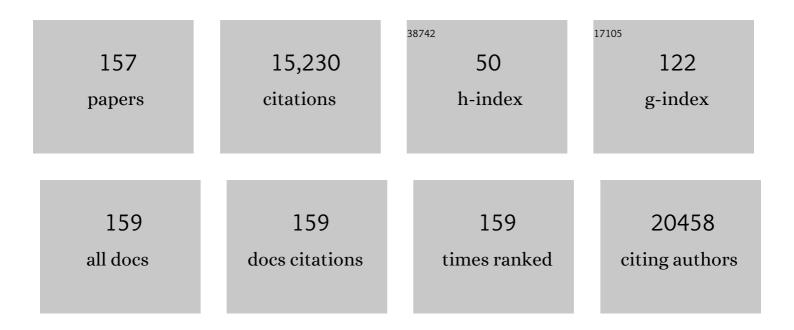
## List of Publications by Year in descending order

Source: https://exaly.com/author-pdf/7043889/publications.pdf Version: 2024-02-01



Let Lut

#	Article	IF	CITATIONS
1	Increasing Solar Absorption for Photocatalysis with Black Hydrogenated Titanium Dioxide Nanocrystals. Science, 2011, 331, 746-750.	12.6	5,359
2	Black titanium dioxide (TiO <sub>2</sub> ) nanomaterials. Chemical Society Reviews, 2015, 44, 1861-1885.	38.1	1,148
3	Toward Efficient Orange Emissive Carbon Nanodots through Conjugated sp <sup>2</sup> â€Domain Controlling and Surface Charges Engineering. Advanced Materials, 2016, 28, 3516-3521.	21.0	583
4	Structural and electronic properties ofh-BN. Physical Review B, 2003, 68, .	3.2	455
5	Titanium Dioxide Nanomaterials: Self-Structural Modifications. Chemical Reviews, 2014, 114, 9890-9918.	47.7	447
6	Properties of Disorder-Engineered Black Titanium Dioxide Nanoparticles through Hydrogenation. Scientific Reports, 2013, 3, 1510.	3.3	317
7	Supra-(carbon nanodots) with a strong visible to near-infrared absorption band and efficient photothermal conversion. Light: Science and Applications, 2016, 5, e16120-e16120.	16.6	237
8	Two-dimensional multibit optoelectronic memory with broadband spectrum distinction. Nature Communications, 2018, 9, 2966.	12.8	211
9	Hydrogenation and Disorder in Engineered Black <mml:math xmlns:mml="http://www.w3.org/1998/Math/MathML" display="inline"&gt;<mml:msub><mml:mi>TiO</mml:mi><mml:mn>2</mml:mn></mml:msub>. Physical Review Letters, 2013, 111, 065505.</mml:math 	7.8	199
10	Probing Charged Impurities in Suspended Graphene Using Raman Spectroscopy. ACS Nano, 2009, 3, 569-574.	14.6	196
11	Atomic structure of the 6H–SiC(0001) nanomesh. Surface Science, 2005, 596, 176-186.	1.9	179
12	Controlled growth of single-walled carbon nanotubes by catalytic decomposition of CH4 over Mo/Co/MgO catalysts. Chemical Physics Letters, 2001, 350, 19-26.	2.6	165
13	Waterâ€Triggered Luminescent "Nanoâ€bombs―Based on Supraâ€(Carbon Nanodots). Advanced Materials, 2015, 27, 1389-1394.	21.0	164
14	FeCl <sub>3</sub> â€Based Few‣ayer Graphene Intercalation Compounds: Single Linear Dispersion Electronic Band Structure and Strong Charge Transfer Doping. Advanced Functional Materials, 2010, 20, 3504-3509.	14.9	154
15	Magnetism in BN nanotubes induced by carbon doping. Applied Physics Letters, 2005, 86, 122510.	3.3	146
16	Stacking-Dependent Optical Conductivity of Bilayer Graphene. ACS Nano, 2010, 4, 4074-4080.	14.6	145
17	Ferromagnetism in GaN:Gd: A Density Functional Theory Study. Physical Review Letters, 2008, 100, 127203 <mml:math <="" td="" xmlns:mml="http://www.w3.org/1998/Math/MathML"><td>7.8</td><td>143</td></mml:math>	7.8	143
18	display="inline"> <mml:mi>p</mml:mi> -Type Conductivity in N-Doped ZnO: The Role of the <mml:math <br="" xmlns:mml="http://www.w3.org/1998/Math/MathML">display="inline"&gt;<mml:msub><mml:mi mathvariant="normal"&gt;N<mml:mi>Zn</mml:mi></mml:mi </mml:msub><mml:mtext mathvariant="normal"&gt;â^^<mml:mi>Zn</mml:mi><mml:mtext mathvariant="normal"&gt;â^^<mml:msub><mml:mi>V</mml:mi><mml:mi< td=""><td>7.8</td><td>143</td></mml:mi<></mml:msub></mml:mtext </mml:mtext </mml:math>	7.8	143

#	Article	IF	CITATIONS
19	From Water Oxidation to Reduction: Transformation from Ni <sub><i>x</i></sub> Co <sub>3–<i>x</i></sub> O <sub>4</sub> Nanowires to NiCo/NiCoO <sub><i>x</i></sub> Heterostructures. ACS Applied Materials & Interfaces, 2016, 8, 3208-3214.	8.0	143
20	Engineering the Electronic Structure of Graphene. Advanced Materials, 2012, 24, 4055-4069.	21.0	141
21	Stacking-Dependent Interlayer Coupling in Trilayer MoS <sub>2</sub> with Broken Inversion Symmetry. Nano Letters, 2015, 15, 8155-8161.	9.1	141
22	Spin-Orbit Splitting in Single-Layer <mml:math <br="" xmlns:mml="http://www.w3.org/1998/Math/MathML">display="inline"&gt;<mml:msub><mml:mi>MoS</mml:mi><mml:mn>2</mml:mn></mml:msub></mml:math> Revea by Triply Resonant Raman Scattering. Physical Review Letters, 2013, 111, 126801.	aled7.8	137
23	Quantum Dot Capped Magnetite Nanorings as High Performance Nanoprobe for Multiphoton Fluorescence and Magnetic Resonance Imaging. Journal of the American Chemical Society, 2010, 132, 14803-14811.	13.7	132
24	Plasma Modified MoS <sub>2</sub> Nanoflakes for Surface Enhanced Raman Scattering. Small, 2014, 10, 1090-1095.	10.0	129
25	Laser-Modified Black Titanium Oxide Nanospheres and Their Photocatalytic Activities under Visible Light. ACS Applied Materials & Interfaces, 2015, 7, 16070-16077.	8.0	122
26	Cu-doped GaN: A dilute magnetic semiconductor from first-principles study. Applied Physics Letters, 2006, 89, 062505.	3.3	121
27	Bandgap engineering of graphene: A density functional theory study. Applied Physics Letters, 2009, 95, .	3.3	121
28	<mml:math <br="" xmlns:mml="http://www.w3.org/1998/Math/MathML">display="inline"&gt;<mml:mi>G</mml:mi></mml:math> -band Raman double resonance in twisted bilayer graphene: Evidence of band splitting and folding. Physical Review B, 2009, 80, .	3.2	116
29	Doped, conductive SiO2 nanoparticles for large microwave absorption. Light: Science and Applications, 2018, 7, 87.	16.6	114
30	Effect of hydrogenation on the microwave absorption properties of BaTiO <sub>3</sub> nanoparticles. Journal of Materials Chemistry A, 2015, 3, 12550-12556.	10.3	108
31	Ferromagnetism in Mg-doped AlN from ab initio study. Applied Physics Letters, 2006, 89, 142501.	3.3	104
32	Strong Microwave Absorption of Hydrogenated Wide Bandgap Semiconductor Nanoparticles. ACS Applied Materials & Interfaces, 2015, 7, 10407-10413.	8.0	104
33	Fabrication of Graphene Nanodisk Arrays Using Nanosphere Lithography. Journal of Physical Chemistry C, 2009, 113, 6529-6532.	3.1	98
34	Electronic Structures and Structural Evolution of Hydrogenated Graphene Probed by Raman Spectroscopy. Journal of Physical Chemistry C, 2011, 115, 1422-1427.	3.1	95
35	Large‣cale Synthesis of Biâ€ŀayer Graphene in Strongly Coupled Stacking Order. Advanced Functional Materials, 2011, 21, 911-917.	14.9	90
36	Bandgap engineering of Cu2CdxZn1â^'xSnS4 alloy for photovoltaic applications: A complementary experimental and first-principles study. Journal of Applied Physics, 2013, 114, .	2.5	88

#	Article	IF	CITATIONS
37	FeNi <sub>3</sub> /NiFeO <i><sub>x</sub></i> Nanohybrids as Highly Efficient Bifunctional Electrocatalysts for Overall Water Splitting. Advanced Materials Interfaces, 2016, 3, 1600368.	3.7	84
38	Hydrogenated black ZnO nanoparticles with enhanced photocatalytic performance. RSC Advances, 2014, 4, 41654-41658.	3.6	81
39	Ferric metal-organic framework for microwave absorption. Materials Today Chemistry, 2018, 9, 140-148.	3.5	75
40	High-Performance Planar-Type Ultraviolet Photodetector Based on High-Quality CH <sub>3</sub> NH <sub>3</sub> PbCl <sub>3</sub> Perovskite Single Crystals. ACS Applied Materials & Interfaces, 2019, 11, 34144-34150.	8.0	71
41	Nonvolatile and Programmable Photodoping in MoTe <sub>2</sub> for Photoresistâ€Free Complementary Electronic Devices. Advanced Materials, 2018, 30, e1804470.	21.0	70
42	ZnO light-emitting devices with a lifetime of 6.8 hours. Applied Physics Letters, 2012, 101, .	3.3	68
43	Broad range energy absorption enabled by hydrogenated TiO <sub>2</sub> nanosheets: from optical to infrared and microwave. Journal of Materials Chemistry C, 2017, 5, 4645-4653.	5.5	64
44	Uniform Mesoporous Anatase–Brookite Biphase TiO <sub>2</sub> Hollow Spheres with High Crystallinity via Ostwald Ripening. Journal of Physical Chemistry C, 2013, 117, 21718-21723.	3.1	59
45	One-pot, large-scale, simple synthesis of Co <sub>x</sub> P nanocatalysts for electrochemical hydrogen evolution. Journal of Materials Chemistry A, 2016, 4, 13011-13016.	10.3	59
46	2D Phosphorene: Epitaxial Growth and Interface Engineering for Electronic Devices. Advanced Materials, 2018, 30, e1802207.	21.0	58
47	Density Functional Theory Study of Finite Carbon Chains. ACS Nano, 2009, 3, 3788-3794.	14.6	56
48	Structure and electronic properties of C <sub>2</sub> N/graphene predicted by first-principles calculations. RSC Advances, 2016, 6, 28484-28488.	3.6	56
49	Performance improvement of amorphous Ga2O3 ultraviolet photodetector by annealing under oxygen atmosphere. Journal of Alloys and Compounds, 2020, 840, 155585.	5.5	54
50	Thermal Dynamics of Graphene Edges Investigated by Polarized Raman Spectroscopy. ACS Nano, 2011, 5, 147-152.	14.6	51
51	Hierarchical 3D dendritic TiO2 nanospheres building with ultralong 1D nanoribbon/wires for high performance concurrent photocatalytic membrane water purification. Water Research, 2013, 47, 4126-4138.	11.3	51
52	Avalanche Gain in Metal–Semiconductor–Metal Ga <sub>2</sub> O <sub>3</sub> Solar-Blind Photodiodes. Journal of Physical Chemistry C, 2019, 123, 18516-18520.	3.1	50
53	Effective hydrogenation of g-C3N4 for enhanced photocatalytic performance revealed by molecular structure dynamics. Applied Catalysis B: Environmental, 2019, 250, 63-70.	20.2	47
54	Reactive Co magic cluster formation onSi(111)â^'(7×7). Physical Review B, 2005, 72, .	3.2	45

#	Article	IF	CITATIONS
55	An experimental and first-principles study on band alignments at interfaces of Cu <sub>2</sub> ZnSnS <sub>4</sub> /CdS/ZnO heterojunctions. Journal Physics D: Applied Physics, 2014, 47, 075304.	2.8	44
56	Functionalizing Single- and Multi-layer Graphene with Br and Br2. Journal of Physical Chemistry C, 2010, 114, 14939-14945.	3.1	43
57	Enhanced Responsivity of Highly Spectrum-Selective Ultraviolet Photodetectors. Journal of Physical Chemistry C, 2012, 116, 1350-1353.	3.1	41
58	A simple tight-binding model for typical graphyne structures. New Journal of Physics, 2012, 14, 113007.	2.9	41
59	Self-powered solar-blind ZnGa2O4 UV photodetector with ultra-fast response speed. Sensors and Actuators A: Physical, 2020, 315, 112354.	4.1	41
60	Configuration-Dependent Interface Charge Transfer at a Moleculeâ <sup>^</sup> Metal Junction. Journal of the American Chemical Society, 2006, 128, 8003-8007.	13.7	38
61	Thickness-dependent energy level alignment of rubrene adsorbed on Au(111). Applied Physics Letters, 2007, 90, 132121.	3.3	38
62	Low temperature edge dynamics of AB-stacked bilayer graphene: Naturally favored closed zigzag edges. Scientific Reports, 2011, 1, 12.	3.3	37
63	Terahertz absorption of hydrogenated TiO2 nanoparticles. Materials Today Physics, 2018, 4, 64-69.	6.0	37
64	Anomalous Broadband Spectrum Photodetection in 2D Rhenium Disulfide Transistor. Advanced Optical Materials, 2019, 7, 1901115.	7.3	37
65	Performance enhancement of a self-powered solar-blind UV photodetector based on ZnGa2O4/Si heterojunction via interface pyroelectric effect. Applied Physics Letters, 2021, 118, .	3.3	37
66	Water-Induced Negative Electron Affinity on Diamond (100). Journal of Physical Chemistry C, 2008, 112, 2487-2491.	3.1	35
67	Shallow Acceptor State in Mg-Doped CuAlO <sub>2</sub> and Its Effect on Electrical and Optical Properties: An Experimental and First-Principles Study. ACS Applied Materials & Interfaces, 2017, 9, 12608-12616.	8.0	35
68	Artificial leaf structures as a UV detector formed by the self-assembly of ZnO nanoparticles. Nanoscale, 2013, 5, 2864.	5.6	34
69	Molecular adsorption induces the transformation of rhombohedral- to Bernal-stacking order in trilayer graphene. Nature Communications, 2013, 4, 2074.	12.8	34
70	Reversible Switching of a Single-Dipole Molecule Imbedded in Two-Dimensional Hydrogen-Bonded Binary Molecular Networks. Journal of Physical Chemistry C, 2014, 118, 1712-1718.	3.1	33
71	From bulk to porous GaN crystal: precise structural control and its application in ultraviolet photodetectors. Journal of Materials Chemistry C, 2019, 7, 14116-14122.	5.5	33
72	The origin of the strong microwave absorption in black TiO2. Applied Physics Letters, 2016, 108, 183102.	3.3	32

#	Article	IF	CITATIONS
73	FUNCTIONALIZATION EFFECT ON THE ELECTRONIC PROPERTIES OF SINGLE WALLED CARBON NANOTUBES. Functional Materials Letters, 2008, 01, 1-6.	1.2	31
74	Dimension induced intrinsic physio-electrical effects of nanostructured TiO2 on its antibacterial properties. Chemical Engineering Journal, 2018, 334, 1309-1315.	12.7	29
75	Ultrafast carrier dynamics in pristine and FeCl3-intercalated bilayer graphene. Applied Physics Letters, 2010, 97, 141910.	3.3	28
76	Wavelength-Tuned Light Emission via Modifying the Band Edge Symmetry: Doped SnO <sub>2</sub> as an Example. Journal of Physical Chemistry C, 2014, 118, 6365-6371.	3.1	28
77	Sub-stoichiometric WO <sub>2.9</sub> for formaldehyde sensing and treatment: a first-principles study. Journal of Materials Chemistry A, 2016, 4, 14416-14422.	10.3	27
78	Band alignments at interface of Cu2ZnSnS4/ZnO heterojunction: An X-ray photoelectron spectroscopy and first-principles study. Journal of Alloys and Compounds, 2015, 628, 293-297.	5.5	26
79	Electronic and optical properties of kesterite Cu2ZnSnS4 under in-plane biaxial strains: First-principles calculations. Physics Letters, Section A: General, Atomic and Solid State Physics, 2013, 377, 2398-2402.	2.1	25
80	A Novel Green TiO <sub>2</sub> Photocatalyst with a Surface Chargeâ€Transfer Complex of Ti and Hydrazine Groups. Chemistry - A European Journal, 2017, 23, 5345-5351.	3.3	25
81	Achieving High-Performance Surface-Enhanced Raman Scattering through One-Step Thermal Treatment of Bulk MoS <sub>2</sub> . Journal of Physical Chemistry C, 2018, 122, 14467-14473.	3.1	25
82	Nucleation of cobalt silicide islands on Si(111)-7 × 7. Journal of Physics Condensed Matter, 2006, 18, 6987-6995.	1.8	24
83	Effect of compressive stress on stability of N-doped p-type ZnO. Applied Physics Letters, 2011, 99, 091908.	3.3	24
84	Structural and electronic properties of4Ãcarbon nanotubes onSi(001)surfaces. Physical Review B, 2006, 74, .	3.2	23
85	Possiblegraphitic-boron-nitride-based metal-free molecular magnets from first principles study. Journal of Physics Condensed Matter, 2006, 18, 569-575.	1.8	23
86	Modulated electrochemical oxygen evolution catalyzed by MoS <sub>2</sub> nanoflakes from atomic layer deposition. Nanotechnology, 2019, 30, 095402.	2.6	22
87	Strong deep-blue photoluminescence of mesographite boron nitride. Journal of Physics Condensed Matter, 2004, 16, 2181-2186.	1.8	21
88	Tunable enhancement of exciton emission from MgZnO by hybridized quadrupole plasmons in Ag nanoparticle aggregation. Applied Physics Letters, 2014, 104, .	3.3	21
89	Bandgapâ€Opened Bilayer Graphene Approached by Asymmetrical Intercalation of Trilayer Graphene. Small, 2015, 11, 1177-1182.	10.0	21
90	Quenching of persistent photocurrent in an oxide UV photodetector. Journal of Materials Chemistry C, 2021, 9, 4039-4045.	5.5	21

#	Article	IF	CITATIONS
91	Structural and Electronic Properties of Inorganic Mixed Halide Perovskites. Physica Status Solidi - Rapid Research Letters, 2018, 12, 1800193.	2.4	19
92	Surface-enhanced Raman of Z-vibration mode in single-walled and multi-walled carbon nanotube. Chemical Physics Letters, 2003, 372, 497-502.	2.6	17
93	Tuning the Electron Affinity and Secondary Electron Emission of Diamond (100) Surfaces by Dielsâ <sup>°,</sup> Alder Reaction. Langmuir, 2007, 23, 9722-9727.	3.5	17
94	Wurtzite NiO: A potential half-metal for wide gap semiconductors. Applied Physics Letters, 2006, 89, 082504.	3.3	16
95	Molecular Orientation and Ordering during Initial Growth of Copper Phthalocyanine on Si(111). Journal of Physical Chemistry C, 2007, 111, 3454-3458.	3.1	16
96	Mechanism of effect of intrinsic defects on electrical and optical properties of Cu <sub>2</sub> CdSnS <sub>4</sub> : an experimental and first-principles study. Journal Physics D: Applied Physics, 2015, 48, 445105.	2.8	16
97	Towards the controlled CVD growth of graphitic B–C–N atomic layer films: The key role of B–C delivery molecular precursor. Nano Research, 2016, 9, 1221-1235.	10.4	16
98	Modifying oxide nanomaterials' properties by hydrogenation. MRS Communications, 2016, 6, 192-203.	1.8	15
99	Speed enhancement of ultraviolet photodetector base on ZnO quantum dots by oxygen adsorption on surface defects. Journal of Alloys and Compounds, 2021, 868, 159252.	5.5	15
100	Conformational degree and molecular orientation in rubrene film by in situ x-ray absorption spectroscopy. Journal of Applied Physics, 2007, 102, 063504.	2.5	14
101	Thickness and stacking geometry effects on high frequency overtone and combination Raman modes of graphene. Journal of Raman Spectroscopy, 2013, 44, 86-91.	2.5	14
102	Performance enhancement of a p-Si/n-ZnGa <sub>2</sub> O <sub>4</sub> heterojunction solar-blind UV photodetector through interface engineering. Journal of Materials Chemistry C, 2021, 9, 10013-10019.	5.5	14
103	Raman scattering investigation of aGe/SiO2/Sinanocrystal system under hydrostatic pressure. Physical Review B, 2004, 69, .	3.2	13
104	Tunable Hybridized Quadrupole Plasmons and Their Coupling with Excitons in ZnMgO/Ag System. Journal of Physical Chemistry C, 2014, 118, 679-684.	3.1	13
105	Zincblende-wurtzite phase transformation of ZnSe films by pulsed laser deposition with nitrogen doping. Applied Physics Letters, 2013, 103, 082111.	3.3	12
106	High-performance flexible UV photodetector based on self-supporting ZnO nano-networks fabricated by substrate-free chemical vapor deposition. Nanotechnology, 2021, 32, 475201.	2.6	12
107	Effects of degree of three-dimensional order and Fe impurities on photoluminescence of boron nitride. Journal of Applied Physics, 2004, 96, 1947-1952.	2.5	11
108	Visible-blind ultraviolet photodetector based on p-Cu2CdSnS4/n-ZnS heterojunction with a type-I band alignment. Journal of Applied Physics, 2016, 120, .	2.5	11

#	Article	IF	CITATIONS
109	Highâ€Throughput Computational Characterization of 2D Compositionally Complex Transitionâ€Metal Chalcogenide Alloys. Advanced Theory and Simulations, 2020, 3, 2000195.	2.8	11
110	Nanocrystalline NiSe <sub>2</sub> /MoS <sub>2</sub> heterostructures for electrochemical hydrogen evolution reaction. Nanotechnology, 2021, 32, 175602.	2.6	11
111	Engineering black titanium dioxide by femtosecond laser filament. Applied Surface Science, 2020, 520, 146298.	6.1	10
112	Raman scattering of germanium nanocrystals embedded in glass matrix under hydrostatic pressure. Journal of Applied Physics, 2003, 93, 9392-9394.	2.5	9
113	Optimized growth of graphene on SiC: from the dynamic flip mechanism. Nanoscale, 2015, 7, 4522-4528.	5.6	9
114	Experimental and first-principles study of photoluminescent and optical properties of Na-doped CuAlO <sub>2</sub> : the role of the Na <sub>Al</sub> -2Na <sub> <i>i</i> </sub> complex. Journal Physics D: Applied Physics, 2015, 48, 335102.	2.8	9
115	Raman scattering study of a GaAsN epitaxial layer. Materials Science in Semiconductor Processing, 2001, 4, 581-584.	4.0	8
116	A tale of two vacancies. Annalen Der Physik, 2011, 523, 129-136.	2.4	8
117	Role of nitrogen-related complex in stabilizing ferromagnetic ordering in a rare-earth and nitrogen codoped ZnO. Ceramics International, 2017, 43, 6013-6018.	4.8	8
118	Raman spectroscopy investigation on excimer laser annealing and thickness determination of nanoscale amorphous silicon. Nanotechnology, 2004, 15, 658-662.	2.6	7
119	First principles study on the interface of CrSbâ^•GaSb heterojunction. Journal of Applied Physics, 2006, 99, 093703.	2.5	7
120	Experimental and theoretical studies on gadolinium doping in ZnTe. Journal of Applied Physics, 2008, 103, .	2.5	7
121	Experimental and first-principles study of ferromagnetism in Mn-doped zinc stannate nanowires. Journal of Applied Physics, 2013, 114, .	2.5	7
122	Effects of magnesium on phosphorus chemical states and <i>p</i> -type conduction behavior of phosphorus-doped ZnO films. Journal of Chemical Physics, 2013, 138, 034704.	3.0	7
123	Dynamical properties and their strain-dependence of ZnSe(ZnSe:N): Zinc-blende and wurtzite. AIP Advances, 2014, 4, .	1.3	7
124	Ti <sub>3</sub> BN monolayer: the MXene-like material predicted by first-principles calculations. RSC Advances, 2017, 7, 11834-11839.	3.6	7
125	MOCVD growth of MgGa2O4 thin films for high-performance solar-blind UV photodetectors. Applied Physics Letters, 2022, 120, .	3.3	7
126	Formation of hydrogenated amorphous carbon films from polymer pyrolysis. Applied Physics A: Materials Science and Processing, 2002, 74, 317-319.	2.3	6

#	Article	lF	CITATIONS
127	Thermal stability of strained Si/Si1â^'xGex heterostructures for advanced microelectronics devices. Thin Solid Films, 2004, 462-463, 76-79.	1.8	6
128	Copper-doped CdTe films with improved hole mobility. Applied Physics Letters, 2007, 91, 092113.	3.3	6
129	Recovering near-band-edge ultraviolet responses in a wide-bandgap oxide with dipole-forbidden bandgap transition. Journal of Alloys and Compounds, 2015, 649, 625-629.	5.5	6
130	n-type Rashba spin splitting in a bilayer inorganic halide perovskite with external electric field. Journal of Physics Condensed Matter, 2018, 30, 265501.	1.8	6
131	The role of sp-hybridized atoms in carbon ferromagnetism: a spin-polarized density functional theory calculation. Journal of Physics Condensed Matter, 2010, 22, 046001.	1.8	5
132	High pressure synthesis and characterization of noble metal nitride IrNx. Materials Letters, 2013, 107, 382-385.	2.6	5
133	Graphene homojunction: closed-edge bilayer graphene by pseudospin interaction. Nanoscale, 2016, 8, 9102-9106.	5.6	5
134	Highly spectrum-selective near-band-edge ultraviolet photodiode based on indium oxide with dipole-forbidden bandgap transition. Ceramics International, 2016, 42, 8017-8021.	4.8	5
135	Giant enhancement of ultraviolet near-band-edge emission from a wide-bandgap oxide with dipole-forbidden bandgap transition. Journal of Alloys and Compounds, 2017, 705, 492-496.	5.5	5
136	Reconstructing the Surface Structure of NaREF <sub>4</sub> Upconversion Nanocrystals with a Novel K <sup>+</sup> Treatment. Chemistry of Materials, 2021, 33, 2548-2556.	6.7	5
137	Single β-Ga <sub>2</sub> O <sub>3</sub> microbelt solar-blind photodetector with high specific detectivity, high rejection ratio and fast speed. Journal Physics D: Applied Physics, 2022, 55, 365107.	2.8	5
138	The Effect of Film Thickness on the C40 TiSi[sub 2] to C54 TiSi[sub 2] Transition Temperature. Journal of the Electrochemical Society, 2005, 152, G754.	2.9	4
139	Control of N/N2 species ratio in NO plasma for p-type doping of ZnO. Journal of Applied Physics, 2011, 110, .	2.5	4
140	A simple rule for finding Dirac cones in bilayered perovskites*. Chinese Physics B, 2019, 28, 077106.	1.4	4
141	Polarity- and Pressure-Dependent Hydrogen Dynamics on ZnO Polar Surfaces Revealed by Near-Ambient-Pressure X-ray Photoelectron Spectroscopy. Journal of Physical Chemistry C, 2020, 124, 25431-25436.	3.1	4
142	Theoretical Study on Structural Stability of Alloy Cages: a Case of Silicon-doped Heterofullerenes. Communications in Computational Physics, 2010, 8, 289-303.	1.7	4
143	High Detectivity of Metal–Semiconductor–Metal Ga <sub>2</sub> O <sub>3</sub> Solar-Blind Photodetector Through Thickness-Regulated Gain. IEEE Transactions on Electron Devices, 2022, 69, 4362-4365.	3.0	4
144	Pressure-dependent band-bending in ZnO: A near-ambient-pressure X-ray photoelectron spectroscopy study. Journal of Energy Chemistry, 2021, 60, 25-31.	12.9	3

#	Article	IF	CITATIONS
145	Point defects: key issues for II-oxides wide-bandgap semiconductors development. Wuli Xuebao/Acta Physica Sinica, 2019, 68, 167802.	0.5	3
146	Raman scattering studies in two kinds of Ge nanosystems under hydrostatic pressure. Physica Status Solidi (B): Basic Research, 2004, 241, 3269-3273.	1.5	2
147	Ultrathin monolayer of rubrene on Au(111) induced by charge transfer. Surface and Interface Analysis, 2011, 43, 1494-1497.	1.8	2
148	High frequency local vibrational modes of oxygen doped CdSe. Journal of Applied Physics, 2013, 114, 194901.	2.5	2
149	The phase transition in PrGa0.95Mg0.05O3 at elevated temperatures. Journal of Physics and Chemistry of Solids, 2009, 70, 533-535.	4.0	1
150	A Density-Functional Study of Oxygen Impurity Complexes in CdTe. AIP Conference Proceedings, 2011, , .	0.4	1
151	Plasma induced deep ultraviolet emissions from MgZnO films. Journal of Luminescence, 2014, 156, 188-191.	3.1	1
152	Low-Temperature-Induced Controllable Transversal Shell Growth of NaLnF4 Nanocrystals. Nanomaterials, 2021, 11, 654.	4.1	1
153	Effect of Al Diffusion on Electrical and Photoluminescent Properties of Mg <sub>x</sub> Zn <sub>1–<i>x</i></sub> O Alloy Films Fabricated on Sapphire Substrates. Nanoscience and Nanotechnology Letters, 2015, 7, 111-116.	0.4	1
154	Stacking dependent optical properties of bilayer graphene. , 2010, , .		0
155	The electronic band structures of gadolinium chalcogenides: a first-principles prediction for neutron detecting. Journal of Physics Condensed Matter, 2016, 28, 185501.	1.8	0
156	Quantum cascade lasers designed toward shorter wavelengths. Journal of Physics Condensed Matter, 2016, 28, 065302.	1.8	0
157	Stretch/Compressâ€Modulated Spin Splitting in Oneâ€Dimensional Melem Chain with a Helical Structure. Physica Status Solidi - Rapid Research Letters, 2019, 13, 1900294.	2.4	Ο